Nitrogen-modified biomass-derived porous carbon for electric double layer capacitors application

Keliang Wang*, Zhengrong Gu* and Qihua Fan*

* South Dakota State University, Brookings, SD, USA, keliang.wang@sdstate.edu, zhengrong.gu@sdstate.edu, qihua.fan@sdstate.edu

ABSTRACT

Rod-shape porous carbon was prepared from aniline modified lignin *via* KOH activation and used as electrode materials for supercapacitors. The specific surface area, pore size and shape could be modulated by the carbonization temperature, which significantly affected the electrochemical performance. Unique rod-shape carbon with massive pores and a high BET surface area of 2265 m^2 g^{-1} were obtained at 700 ºC in contrast to irregular morphology created at other carbonization temperatures. In 6 mol L^{-1} KOH electrolyte, a specific capacitance of 336 F g^{-1}, small resistance of 0.9 Ω and stable charge/discharge at current density of 1 A g^{-1} after 1, 000 cycles were achieved using rod-shape porous carbon as electrodes in an electrical double layer capacitor.

Keywords: biomass, porous carbon, lignin, activation, supercapacitor

1 INTRODUCTION

Supercapacitors, also known as electrochemical capacitors have received considerable attention because of their high power density, fast charge/discharge capability and long cycle life [1-3]. Supercapacitors can be classified into two major categories based on the energy storage mechanism: electrical double layer capacitor (EDLC) and pseudocapacitor [4]. Energy stored in an EDLC is proportional to the electrostatic charge accumulated at the electrode/electrolyte interface. Therefore, the specific capacitance depends on the electrode surface area accessible to the electrolyte. On the other hand, pseudocapacitors store energy *via* the Faradaic reactions that occurr between the electrode materials and electrolyte. Pseudocapacitors usually use metal oxides/hydroxides (*e.g.* MnO_2, NiO, $Ni(OH)_2$, Co_3O_4) electrodes and possess higher specific capacitance than EDLCs that use carbon as electrode materials [5-9]. Pseudocapacitors are expected to find broader applications if their cycle stability can be improved, electrical conductivity can be increased, and the material cost can be reduced [10, 11].

Carbon-based materials are the primary electrode materials for EDLC. Porous carbon, such as activated carbon (AC), mesoporous carbon and graphene [12-14] have been commonly used in EDLC. EDLC electrode materials should possess the following characteristics: i) high specific surface area (SSA) that provides sufficient accessible surface to the electrolyte; ii) proper pore size that allows the electrolyte ions to transfer smoothly with short diffusion pathways; iii) excellent electrical conductivity to minimize resistive loss during charge/discharge; iv) sustainable and wide availability with low cost. The preparation of mesoporous carbon usually involves complex synthetic procedures in most cases, while graphene suffers from high cost although it could be obtained in labs after a series of harsh chemical treatments. Alternatively, activated carbon derived from abundant, renewable biomass feedstock can be produced sustainably at low cost [15]. So far, carbon materials derived from biomass such as rice husk, coffee grounds, grape seed, cornstalk, banana peel [16-20], have been explored as electrode materials in EDLC and promising electrochemical performance has been demonstrated.

Recent research showed that introducing nitrogen into activated carbon could induce additional pseudo-capacitance *via* reversible redox reactions and improve the wettability between the electrodes and electrolytes [21]. As a result, the capacitance performance of EDLC was greatly promoted. Therefore, biomass derived carbon materials with nitrogen may be promising electrode materials for EDLC. Since biochar typically contains low nitrogen content, we hypothesize that combination of nitrogen rich compounds with biomass will lead to biochar with high nitrogen content. Furthermore, there may be opportunities to tune the physicochemical properties of the nitrogen rich biochar, such as morphology, surface area, and conductance. Regarding the source of nitrogen, aniline appears a promising candidate because it is easy to polymerize, and the polymer can be grown into different shapes such as wires, tubes and spheres [22-24] by controlling the synthetic conditions.

Herein, we present aniline modified lignin as the raw materials to prepare rod-shape porous carbon as EDLC electrode materials. It is shown that the chemical activation plays a key role in achieving large SSA, uniform pore size distribution and good conductivity, which lead to excellent electrochemical performance.

2 EXPERIMENTAL

2.1 Preparation of activated carbon

The mixture of olvent lignin (3 g), aniline (1.5 ml) and 30 ml ethanol were dried at 80 ºC . Then it was heated at 400 ºC for 1 h in a muffle furnace under the protection of

nitrogen. Then, it was mixed with potassium hydroxide (KOH) in a mass ratio of 1:3, in a steel crucible. The crucible was placed in an oven and dried at 110 ºC for 24 h. Then, the crucible was transferred into a muffle and activated at 600 ~900 ºC for 1 h under N_2 protection. Afterwards, the carbonized solids were washed and then dried at 105 ºC overnight in an oven. The carbonized samples were denoted as PL-600, PL-700, PL-800 and PL-900. In addition, the carbon material derived from lignin (L) with the same method at 700 ºC but without KOH was used as control sample.

2.2 Physical and electrochemical characterization

X-ray photoelectron spectroscopy (XPS), raman spectra, isothermal adsorption analyses, elemental analysis and transmission electron microscope (TEM) were used to characterize the structure, ingredient and morphology of prepared samples. Cyclic voltammetry (CV) and electrochemical impedance spectroscopy tests were measured on an electrochemical work station. The galvanostatic charge/discharge curves were obtained from a battery test system.

3 RESULTS AND DISCUSSION

TEM images of PL-700 with different magnifications are shown in Fig. 1. In contrast to the chunk shape for the L sample, this PL-700 material has rod-shape morphology (Fig. 1a and b) with large amount of pores. In high resolution images (Fig. 1c and d), the pores with different size can be observed clearly. The pores were closely distributed in the surface, but not connected with each other. The walls were so thin that it was damaged when irradiated by TEM beam.

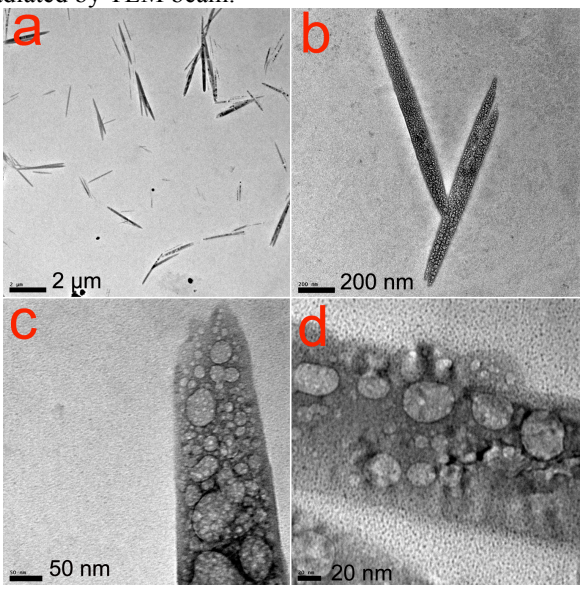

Fig. 1 Different magnifications TEM images of PL-700.

Meanwhile, pores were also observed in samples PL-600, PL-800, and PL-900. Different from PL-700, the pores in the other samples were obviously aggregated. This difference in the morphology of the activated carbon samples was primarily due to the activation temperature. Aniline monomer can be easily polymerized, and polyaniline can grow into different shapes, such as rods or spheres, even at room temperature. At high temperatures, the activation agent KOH reacted with carbon, producing gases (CO, H_2O and CO_2), forming pores and leaving behind potassium salts (K, KOH and K_2CO_3) [25]. The interconnected cavities in the porous carbon might serve as reservoirs for the electrolyte, Thus, the pores with different size provided channels for ion transport and the thin walls led to short transport distance, resulting in small inner pore ions transferring resistance [26]. These characteristics were expected to promote the supercapacitor performance, as will be discussed later. In addition, elemental mapping was performed and shown a homogeneous distribution of elements (C, N and O) in all activated samples.

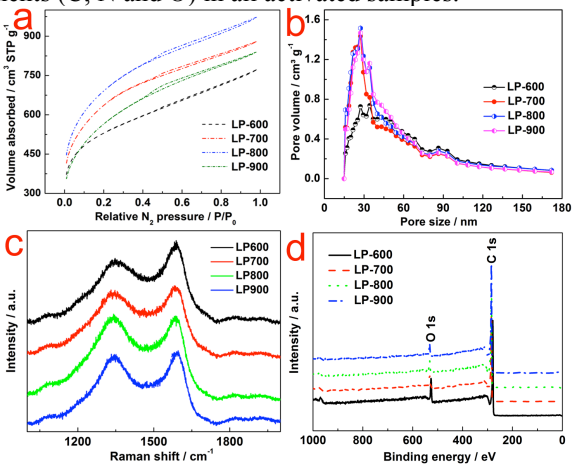

Fig. 2 N_2 sorption-desorption isotherms (a) and pore size distribution (b), Raman spectra (c) and XPS survey spectra (d) of PL-600, PL-700, PL-800, and PL-900.

N_2 sorption/desorption was conducted to characterize the surface area and pores size distribution (Fig. 2a and b). The BET SSA were 1886, 2265, 2467, and 2014 $m^2 g^{-1}$ for samples PL-600, PL-700, PL-800 and PL-900, respectively, and showed dependence on the activation temperature. Interestingly, the pore size distribution (Fig. 2 b) for all the samples showed similar pore width centered at 27 nm. The similar pore structure was probably resulted from using the equal amount of KOH and biomass for all samples activation. The samples possessed higher BET SSA with proper pore sizes are expected to be a promising EDLC electrode material. Raman spectra of the samples are shown in Fig. 2c. Two apparent peaks in the spectra were found, corresponding to the *D* band at 1346 cm^{-1} and *G* band at 1585 cm^{-1}. The *G* band revealed the formation of graphitic carbon. The *D* band reflected the degree of disorder which was associated with defects in hexagonal graphitic layers. The relative intensity ratio of *D* and G bands (I_D/I_G) was also used to evaluate degree of crystallinity, the smaller value means the higher degree of

graphitization and less disordered nature of carbon [27, 28]. The I_D/I_G values were estimated to be 1.33, 1.10, 1.07 and 1.04 for the samples activated at 600 ºC , 700 ºC , 800 ºC and 900 ºC , respectively. The values decreased as the temperature increased, indicating the degree of graphitization was enhanced and electrical conductivity would be promoted. To clarify the surface chemical compositions of the obtained samples, XPS measurement was employed. As expected, C (285 eV), O (532 eV) signals were detected, however, no N signal was detected in the XPS survey spectra for all four samples (Fig. 2d). This result appeared inconsistent with the results of element mapping in TEM and given the N-containing raw material we used. Elemental analysis was subsequently carried out to analyze the compositions of the samples. As presented, N was indeed detected along with C and O in all four samples. The content of N was found to be 0.64 *wt*%, 0.29 *wt*%, 0.26 *wt*% and 0.33 *wt*% for PL-600, PL-700, PL-800, and PL-900, respectively. Considering the XPS result, it was likely that N was accumulated below the surface because this surface analysis technique had a detection depth only ca. 10 nm. Introducing nitrogen into activated carbon has proven to be effective in improving the conductivity and subsequently promoting the capacitance performance [29]. Therefore, it is important to confirm the existence of nitrogen. The presence of N was expected to induce additional pseudo-capacitance *via* reversible redox reactions and improve the wettability between the electrodes and electrolytes [21].

To evaluate the specific capacitance in the two-electrode system, the following equation [31] was used:

$$C = \frac{I\Delta t}{\Delta V M} \times 4 \qquad (1)$$

where C (F g^{-1}) is the specific capacitance, I (A) is the discharge current, Δt (s) is the discharge time, Δv (V) is the voltage change (excluding the *iR* drop) within the discharge time, and M (g) is the total mass of the active materials on the two electrodes, factor 4 is to adjust the capacitance of the cell and the combined mass of two electrodes to the capacitance and mass of a single electrode.

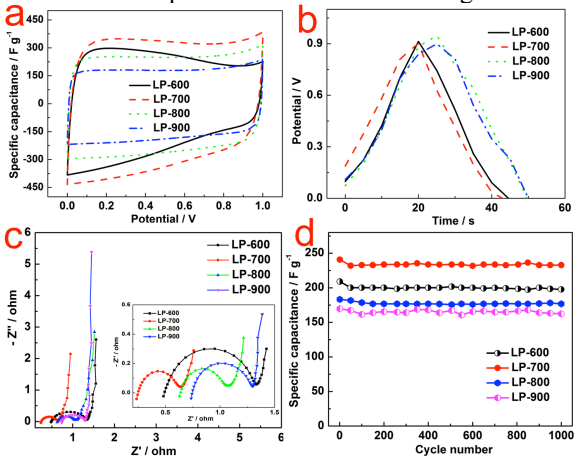

Fig. 3 CV curves (a) at scanning rate 20 mV s^{-1}, galvanostatic charge/discharge (b) nyquist plots (c) and cycle life (d) of PL-600, PL-700, PL-800 and PL-900 electrodes in 6 mol L^{-1} KOH electrolyte.

Fig. 3a showed the CV curves of PL-600, PL-700, PL-800, and PL-900 at a scanning rate of 20 mV s^{-1}. The CV curves tended to be regular rectangle with the increase in the activation temperature, indicating materials have promising potential as EDLC electrodes. The sample PL-700 exhibited the largest specific capacitance of 333 F g^{-1}, which was significantly larger than that of 21, 269, 247, 179 F g^{-1} for L, PL-600, PL-800 and PL-900, respectively. In addition, PL-700 behaved better than PL-600, PL-800 and PL-900 at different scanning rates (5, 10, 20, 50, 100 and 200 mV s^{-1}). Although PL-700 exhibited the highest specific capacitance among these four samples, it was not the sample with the largest SSA or N content. This seems not in consistent with the expected contribution from N and porous structure. The most possible reason was that the PL-700 sample had larger effective SSA that provided better accessibility to the electrolyte and facilitated efficient ion transport with lower resistance [30]. The galvanostatic charge/discharge curves of activated electrodes at current density of 1.0 A g^{-1} was shown in Fig. 3b. As other samples, PL-700 also displayed a symmetric triangle curve and no obvious Ohmic drop (IR_{drop}) was observed, which was an indicative of good capacitive performance [31].

Impedance was considered as an important index to access the electrode materials for EDLC. The EIS measurement was performed in the range from 0.1 to 100 kHz in the two-electrode cell to characterize the resistance (as shown in Fig. 3c). At the low frequency region, a straight line could be observed, which represented the contact resistance. The steeper line indicates better behavior of the electrodes [32]. In the high frequency region, all the samples exhibited an obvious semicircle for which the smaller radius means the lower ESR (inset in Fig. 3c). This behavior indicates equivalent series resistance (ESR) referring to electrode conductivity and the charge-transfer resistance in the electrode materials. The PL-700 exhibited the steepest straight line and smallest radius at low and high frequencies, demonstrating the excellent electrochemical characteristics. The cyclic stability of the electrodes was measured by charge/discharge at a constant current density of 1.0 A g^{-1}, as shown in Fig. 3d. After 1, 000 charge/discharge cycles, all the samples showed almost 100% retention of capacitance. Still, PL-700 maintained the largest specific capacitance and steady cycle life compared to other samples. Therefore, it was a very promising EDLC electrode material.

4 CONCLUSION

The rod-shape porous carbon derived from aniline modified lignin has been successfully prepared *via* KOH activation. The activation temperature determines the microstructure and morphology of the resulting carbon. The materials activated at 700 ºC exhibited high SSA with in-

connected cavities, which lead to the highest specific capacitance of 336 F g^{-1}, smallest resistance of 0.9 Ω and excellent stability in electrochemical performance as compared to the materials activated at different temperatures (600, 800, and 900 ºC). The PL-700 also exhibited remarkable operational characteristics in terms of power and energy density. The superior performance of PL-700 indicates that it is a promising electrode material for EDLC.

Acknowledgement

This research was funded by China Scholarship Council, USDA-NIFA 2011-67009-20030, NSF EPSCoR Track II Dakota BioCon center #1330840, NSF award #1462389, NSF CHE-0840507 and NSF award #1536209.

5 REFERENCES

[1] M. Zhi, C. Xiang, J. Li, M. Li, N. Wu, Nanoscale 5 72-88, 2013.
[2] S. Faraji, F.N. Ani, Sust. Energ. Rev. 42, 823-834, 2015.
[3] N. Devillers, S. Jemei, M.-C. Péra, D. Bienaimé, F. Gustin, J. Power Sources 246, 596-608, 2014.
[4] S. Faraji, F.N. Ani, , J. Power Sources 263, 338-360, 2014.
[5] J. Yan, Z. Fan, W. Sun, G. Ning, T. Wei, Q. Zhang, R. Zhang, L. Zhi, F. Wei, Adv. Fun. Mater., 22, 2632-2641, 2012.
[6] Y. He, W. Chen, X. Li, Z. Zhang, J. Fu, C. Zhao, E. Xie, ACS nano 7, 174-182, 2012.
[7] X.-h. Xia, J.-p. Tu, Y.-q. Zhang, Y.-j. Mai, X.-l. Wang, C.-d. Gu, X.-b. Zhao, Rsc Adv. 2, 1835-1841, 2012.
[8] S. Vijayakumar, S. Nagamuthu, G. Muralidharan, ACS Appl. Mater. Inter. 5, 2188-2196, 2013.
[9] H. Jiang, J. Ma, C. Li, Chem. Comm. 48, 4465-4467, 2012.
[10] B.P. Bastakoti, Y. Kamachi, H.S. Huang, L.C. Chen, K.C.W. Wu, Y. Yamauchi, Eur. J. Inorg. Chem. 2013 39-43, 2013.
[11] C. Largeot, C. Portet, J. Chmiola, P.-L. Taberna, Y. Gogotsi, P. Simon, J. Am. Chem. Soc. 130, 2730-2731, 2008.
[12] M. Chen, X. Kang, T. Wumaier, J. Dou, B. Gao, Y. Han, G. Xu, Z. Liu, L. Zhang, J. Solid State Electr. 17, 1005-1012, 2013.
[13] Y. Huang, J. Liang, Y. Chen, Small 8, 1805-1834, 2012.
[14] J. Wei, D. Zhou, Z. Sun, Y. Deng, Y. Xia, D. Zhao, Adv. Fun. Mater. 23, 2322-2328, 2013.
[15] O. Ioannidou, A. Zabaniotou, Renew. Sust. Energ. Rev. 11, 1966-2005, 2007.
[16] L. Wang, G. Mu, C. Tian, L. Sun, W. Zhou, P. Yu, J. Yin, H. Fu, ChemSusChem 6, 880-889, 2013.
[17] M. Zhi, F. Yang, F. Meng, M. Li, A. Manivannan, N. Wu, ACS Sust. Chem. Eng. 2, 1592-1598, 2014.
[18] D. Jiménez-Cordero, F. Heras, M.A. Gilarranz, E. Raymundo-Piñero, Carbon 71, 127-138, 2014.
[19] Y.S. Yun, M.H. Park, S.J. Hong, M.E. Lee, Y.W. Park, H.-J. Jin, ACS Appl Mater. & Inter. 7, 3684-3690, 2014.
[20] X. He, P. Ling, M. Yu, X. Wang, X. Zhang, M. Zheng, Electrochim. Acta 105, 635-641, 2013.
[21] W. Si, J. Zhou, S. Zhang, S. Li, W. Xing, S. Zhuo, Electrochim Acta 107, 397-405, 2013.
[22] Z. Cai, L. Li, J. Ren, L. Qiu, H. Lin, H. Peng, J. Mater. Chem. A 1, 258-261, 2013.
[23] R.C.Y. King, F. Roussel, J.-F. Brun, C. Gors, Synthetic Met. 162, 1348-1356, 2012.
[24] J. Han, G. Xu, B. Ding, J. Pan, H. Dou, D.R. MacFarlane, J. Mater. Chem. A 2, 5352-5357, 2014.
[25] J. Wang, S. Kaskel, J. Mater. Chem. 22, 23710-23725, 2012.
[26] C. Ruan, K. Ai, L. Lu, RSC Adv. 4, 30887-30895, 2014.
[27] S. Shanmugam, T. Osaka, Chem. Commun. 47, 4463-4465, 2011.
[28] L.-F. Chen, Z.-H. Huang, H.-W. Liang, W.-T. Yao, Z.-Y. Yu, S.-H. Yu, Energ. & Environ. Sci. 6, 3331-3338, 2013.
[29] B. Zheng, J. Wang, F.-B. Wang, X.-H. Xia, Electrochem. Commun. 28, 24-26, 2013.
[30] L. Zhang, F. Zhang, X. Yang, G. Long, Y. Wu, T. Zhang, K. Leng, Y. Huang, Y. Ma, A. Yu, Sci. Rep.3 2013.
[31] Q. Wu, Y. Xu, Z. Yao, A. Liu, G. Shi, ACS nano, 4, 1963-1970, 2010.
[32] X. Hong, K. Hui, Z. Zeng, K. Hui, L. Zhang, M. Mo, M. Li, Electrochim. Acta 130, 464-469, 2014.